Surface Deformation Monitoring and Subsidence Mechanism Analysis in Beijing based on Time-series InSAR

Wang JingHui [1,2,3], Luo ZiYan[4*], Zhou Lv[4,5], Li Xinyi[4], Wang Cheng[4], Qin Dongming[4]
[1] Mineral Resources Exploration Center of Henan Geological Bureau, Zhengzhou 450012, China
[2] Henan Remote Sensing Intelligent Monitoring Engineering Technology Research Center for Satellite, Aircraft and Land Survey, Zhengzhou 450006, China
[3] Henan Natural Resources Science and Technology Innovation Center (Research on Remote Sensing Intelligent Monitoring for Satellite, Aircraft and Land Survey) , Zhengzhou 450000, China
[4] College of Geomatics and Geoinformation, Guilin University of Technology, Guilin 541006, China
[5] Key Laboratory of China-ASEAN Satellite Remote Sensing Applications，Ministry of Natural Resources of the People's Republic of China, Nanning 530221, China

KEY WORDS: Beijing; Time-Series InSAR; Surface Deformation Monitoring; Land Subsidence; Mechanism of Subsidence formation

ABSTRACT:
This article uses 43 Sentinel-1A image datasets covering Beijing to obtain time series surface deformation information in the study area from January 2022 to October 2023. It analyzes the causes of land subsidence by integrating precipitation and urban construction. The main research results are as follows: (1) Three distinct subsidence areas are identified in the eastern part of Chaoyang District in Beijing (Subsidence Area A), the northwestern part of Tongzhou District in Beijing (Subsidence Area B), and Yanjiao Town in Hebei Province (Subsidence Area B), which is adjacent to Beijing. Subsidence Areas A and B exhibit a dispersed pattern, with maximum land subsidence rates exceeding −30 mm/year. In contrast, Subsidence Areas C displays a funnel-shaped subsidence, where the majority of areas experience land subsidence rates exceeding −25 mm/year, with a maximum rate reaching −45 mm/year. (2) Precipitation has a significant impact on surface deformation in the study area, and there is a strong correlation between precipitation and land subsidence, with correlation values of 0.77, 0.77, and 0.74, respectively. (3) Urban construction has a certain impact on land subsidence, but the degree of impact varies in different regions.

1. Introduction

Land subsidence is a widely distributed geological disaster phenomenon on a global scale. Timely acquisition of the state of land subsidence is of great significance in preventing potential economic and property losses and threats to people's lives caused by land subsidence.

Land subsidence is a widespread geological phenomenon globally. The timely acquisition of information on land subsidence is of great significance for preventing potential economic and property losses, as well as mitigating threats to people's lives caused by this geological hazard (Bagheri et al., 2021). Traditional surface deformation monitoring techniques include Global Navigation Satellite System (GNSS) measurements, bedrock measurements and levelling measurements. However, these methods have various drawbacks such as a limited monitoring range and high monitoring costs (Wang, 2001). With the development of Interferometry Synthetic Aperture Radar (InSAR) technology, obtaining high-precision surface deformation information over a large range using SAR image data has become possible (Bamler and Hartl, 1998). Time-series InSAR has the advantages of all-weather and high accuracy, making up for the shortcomings of traditional surface deformation monitoring techniques (Ferretti et al., 2001; Berardino et al., 2002). The SBAS-InSAR technology in time-series InSAR technology is widely used in urban land subsidence monitoring cases due to its unique characteristics (Zhou et al., 2016).

Located in the north of North China Plain, Beijing serves as the capital of China. By the end of 2022, the permanent population of Beijing will reach 21.843 million. Beijing is one of the cities with severe land subsidence in China. Historical data indicates that land subsidence in Beijing has been progressively intensifying since the 1950s (Chen et al., 2015; Chen et al., 2016). Although the prevention and control of land subsidence in Beijing has been effective in recent years, it still poses a huge threat to the safety of people's lives and property in Beijing. The problem of land subsidence in Beijing is still a geological hazard that cannot be ignored (Sheng et al., 2023)

This study uses SBAS-InSAR technology to monitor recent surface deform employs ation in Beijing. By utilizing 43 Sentinel-1 SAR images that cover Beijing, we obtained time-series surface deformation information from January 2022 to October 2023. The mechanism of land subsidence in the study area is analyzed by integrating data on precipitation and urban construction.

2. Study Area and Data Sources

2.1 Study Area

Beijing is located in the north of the North China Plain, with longitude and latitude ranging from 115°42′E to 117°24′E, 39°24′N to 41°36′N, and a total area of 16,410.54 km² . The overall terrain of Beijing is higher in the northwest and lower in the southeast, with an average elevation of 43.5m. The northwest direction of Beijing is surrounded by the branches of the Taihang Mountains and the western section of the Yanshan Mountains, while the southeast direction is the mountain front impact plain formed by rivers such as the Yongding River and Chaobai River. As shown in Figure 1, the blue-boxed area represents the study area of this article, which includes a small portion of mountainous terrain, but overall it is mainly plain terrain. The study area covers most of Beijing and some parts of Hebei Province.

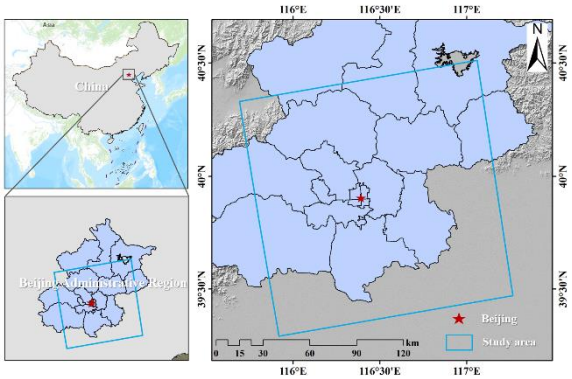

Figure 1. Geographical location of the study area (The study area is in the blue box)

2.2 Data Sources

This study is based on SBAS InSAR technology and uses 43 Sentinel-1A SAR images provided by the European Space Agency (ESA) covering the study area to obtain surface deformation information from January 2022 to October 2023. The main parameters of Sentinel-1A SAR images are shown in Table 1. This study used precision orbit numbers published by ESA to perform orbit refinement and phase re-flattening for all image data, and used DEM data at a resolution of 30 meters provided by the National Aeronautics and Space Administration (NASA) to remove terrain phase errors. In addition, this article also used precipitation data published by the Beijing Water Bureau and ArcGIS historical optical images (https://livingatlas.arcgis.com/wayback) to analyze the mechanism of land subsidence.

Parameter	Value
Product type	Sentinel-1A
Wavelength	C (5.63 cm)
Beam mode	IW
Revisit period	12 days
Polarization	VV
Time range	2022.01–2023.10
Orbit direction	Ascending
Incidence angle	39.6°
Resolution	5m×20m

Table 1 The main parameters of Sentinel-1A SAR images

3. Methodology

3.1 Time-series InSAR technology

SBAS-InSAR technology is a commonly used time-series InSAR technology, originally proposed by Berardino et al. (2002). SBAS-InSAR technology is often applied in large-scale monitoring cases in cities. The basic principle is to select a pair of small temporal and spatial baseline connections based on the distribution of SAR data images, In order to generate interferograms and ensure minimal loss of decoherence and terrain phase errors. Then conduct time-series analysis to obtain time-series information on surface deformation. M interferograms are generated from $N+1$ SAR image data, and there is a certain correlation between M and N. The specific constraint relationship between the two is as follows (Colesanti et al., 2003):

$$\frac{N+1}{2} \le M \le N\frac{N+1}{2} \tag{1}$$

Generate the i-th differential interferogram within the time range t_A and t_B, and the phase corresponding to any pixel in a differential interferogram can be represented as:

$$\begin{aligned}\delta\phi_i(x,r) &= \phi(t_B,x,r) - \phi(t_A,x,r) \\ &\approx \frac{4\pi}{\lambda}[d(t_B,x,r) - d(t_A,x,r)] + \Delta\phi^i_{topo}(x,r) \\ &+\Delta\phi^i_{atm}(x,r) + \Delta\phi^i_{noise}(x,r)\end{aligned} \tag{2}$$

In the formula, $\phi(t_A,x,r)$ and $\phi(t_B,x,r)$ represent the phase values at coordinates (x,r) at t_A and , respectively. $\Delta\phi^i_{topo}(x,r)$ represents residual terrain phase in differential interferograms, $\Delta\phi^i_{atm}(x,r)$ represents atmospheric delay phase, and $\Delta\phi^i_{noise}(x,r)$ represents decoherence noise phase. In the presence of DEM data, terrain phase can be simulated to remove terrain phase errors (Fattahi et al., 2013). The phase of all differential interferograms is represented as a matrix $\delta\phi$,and the average surface deformation rate is represented by matrix V . There is a relationship between matrix $\delta\phi$ and matrix V as follows:

$$BV = \delta\phi \tag{3}$$

The size of matrix B is related to M and N, and in general, the B matrix is rank deficient. Singular value decomposition (SVD) is commonly used for rank defect solving, so the acquisition of surface deformation information in time-series is based on the process of jointly solving multiple baseline sets using SVD to obtain the least squares norm solution (Tao et al., 2020).

3.2 Time-series InSAR Data Processing

The data processing flow of SBAS InSAR is shown in the following Figure 2, which can be roughly divided into four parts. The same color represents the small steps in the same big step, and the gray steps represent the input of data and the final obtained time-series surface deformation information.

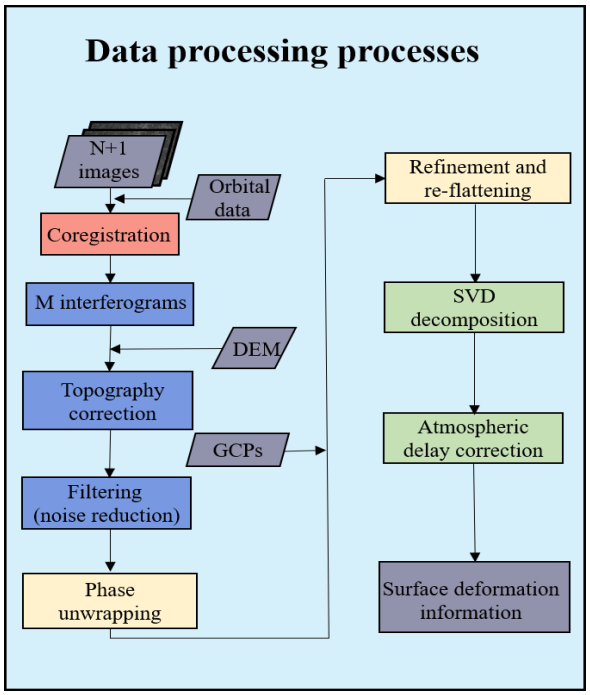

Figure 2. Time-series InSAR processing flow

(1) Use the Sentinel-1A SAR image collected on January 13, 2023 as the main image to register and resample the secondary images. Set appropriate time and space thresholds to avoid generating small baseline sets due to decoherence. During data processing, a time baseline threshold of 60 days and a spatial baseline threshold of 2% were set, resulting in 274 pairs of connected image pairs. The spatiotemporal baseline generated by connecting the main and secondary images is shown in Figures 3 and 4.

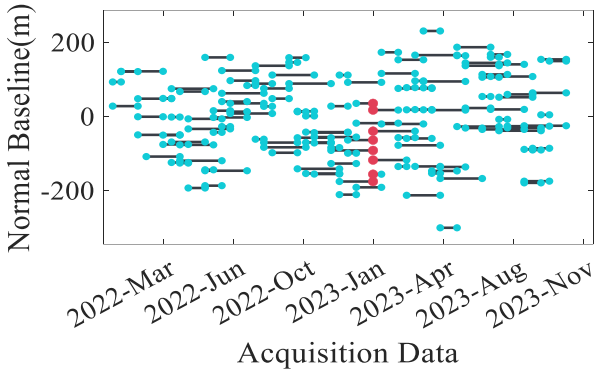

Figure 3. Time–position baseline of Sentinel-1 image interferometric pairs (The red dots represent the main image)

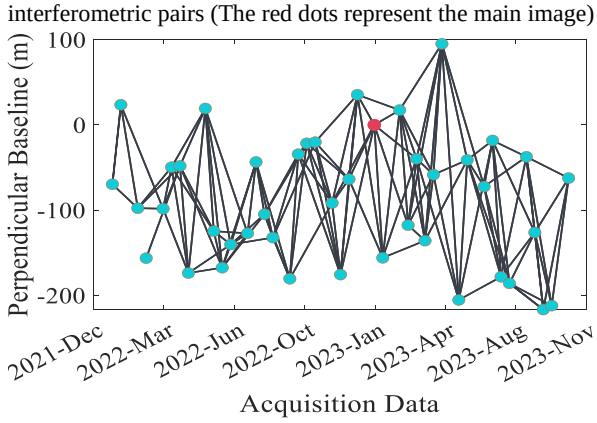

Figure 4. Time–baseline of Sentinel-1 image interferometric pairs (The red dot represent the main image)

Based on 274 pairs of connected differential interferograms, Goldstein filtering is used to process interference fringes to reduce phase incoherence noise caused by spatial or temporal baselines. Use 30 meter resolution DEM data to remove terrain phase from the filtered interferogram.

(2) Based on 274 pairs of connected differential interferograms, Goldstein filtering is employed to process interference fringes, reducing phase decoherence noise caused by spatial or temporal baselines. Subsequently, 30-meter resolution DEM data is utilized to eliminate terrain phase from the filtered interferogram.

(3) Phase unwrapping is based on interferograms, with the aim of restoring the blurred full cycle phase 2π. The threshold for phase unwrapping is set to 0.2. Select time-series stable points as ground control points based on interferograms, correlation coefficient images, and external DEMs. Then use ground control points for orbit refinement and phase re-flattening, with the aim of removing phase ramps that still exist after unwinding.

(4) By establishing observation equations using the Singular Value Decomposition (SVD) method and obtaining the least squares norm solution, the time-series surface deformation information in the study area can be retrieved. Subsequently, nonlinear surface deformation and atmospheric phase errors within the time-series surface deformation data are reduced through time-domain and spatial-domain filtering.

4. Result

4.1 Results of surface deformation in the study area

This paper processes 43 Sentinel-1A SAR images covering the study area using SBAS-InSAR technology, acquiring time-series surface deformation information along the Line of Sight (LOS) direction from January 2022 to October 2023. The surface deformation rate of the study area is depicted in Figure 5.

Three distinct areas of significant land subsidence were observed in the eastern part of the study area. These areas of pronounced land subsidence phenomena are marked as Areas A, B, and C. Area A, centered around Jinzhan Township in Chaoyang District, Beijing, also includes parts of the Tongzhou District. The annual average land subsidence rate in this area is around −20 mm/year, with the maximum land subsidence rate reaching −32 mm/year. Subsidence Area B is located in the western part of Tongzhou District, Beijing. The more severely affected areas are Liyuan Town and Taihu Town. The land subsidence in this area is relatively scattered and shows a trend of outward expansion. The annual average land subsidence rate in this area exceeds −20 mm/year, with the maximum land subsidence rate reaching −35 mm/year. Subsidence Area C is located in Yanjiao Town, Hebei Province, bordering Beijing. The land subsidence in this area is distinctly represented as a land subsidence funnel, with an annual average surface deformation rate exceeding −25 mm/year and the maximum land subsidence rate reaching −45 mm/year. In the study area, other regions exhibit relatively stable surface deformation, with the majority of these areas showing surface deformation rates ranging from −10 mm/year to 10 mm/year.

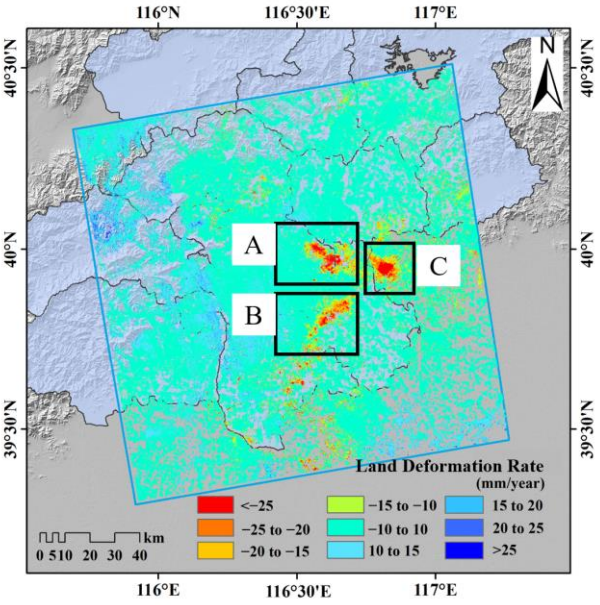

Figure 5. Surface deformation rate in the study area

Feature points at the centers of the three subsidence areas were selected and named after their respective locations: CY point for Chaoyang District, TZ point for Tongzhou District, and YJ point for Yanjiao Town, as depicted in Figure 6. Time-series surface deformation at the feature points in the land subsidence centers (Figure 7) indicates that the land subsidence conditions in Subsidence Area A and Subsidence Area B are similar. The surface deformation curves show a slow trend, with instances of land subsidence recovery observed during the study period, and the cumulative surface deformation in both areas exceeds −40 mm. Subsidence Area C experiences the most severe land subsidence, with steeper surface deformation curves and a maximum cumulative land subsidence at the center reaching −75 mm.

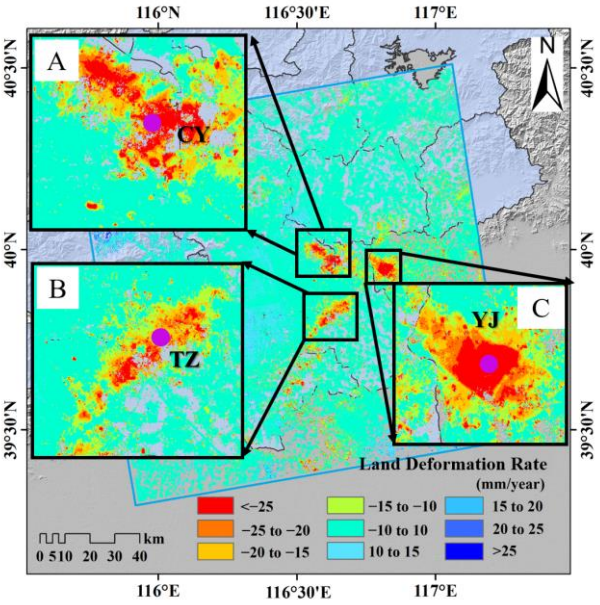

Figure 6. Location of surface deformation feature points

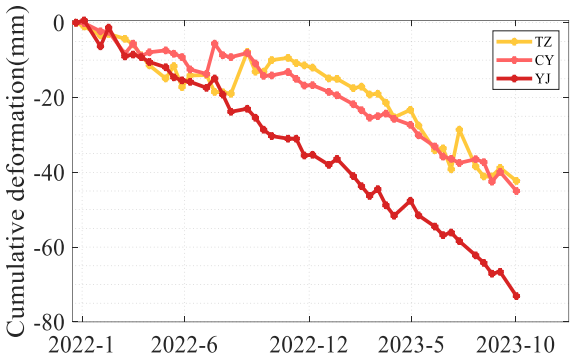

Figure 7. Time series surface deformation curves of three feature points

4.2 **Precision Validation of Surface Deformation in the Study Area**

This paper evaluates the accuracy of InSAR monitoring results within the study area using RMSE data. The spatial distribution of the Root Mean Square Error (RMSE) within the study area is shown in Figure 8. Most areas within the study region exhibit low RMSE values, while the peripheral regions may have higher RMSE values due to unwrapping errors. This paper conducts a statistical analysis of the Root Mean Square Error (RMSE) values within the study area. Figure 9 displays the frequency distribution histogram of the RMSE values. The histogram indicates that the majority of RMSE values are distributed in the range of 2 mm/year to 3 mm/year, with points having RMSE values less than 10 mm/year accounting for 99.47% of all RMSE data points. The overall results indicate that the time-series surface deformation data acquired using SBAS-InSAR for the study area demonstrate good reliability.

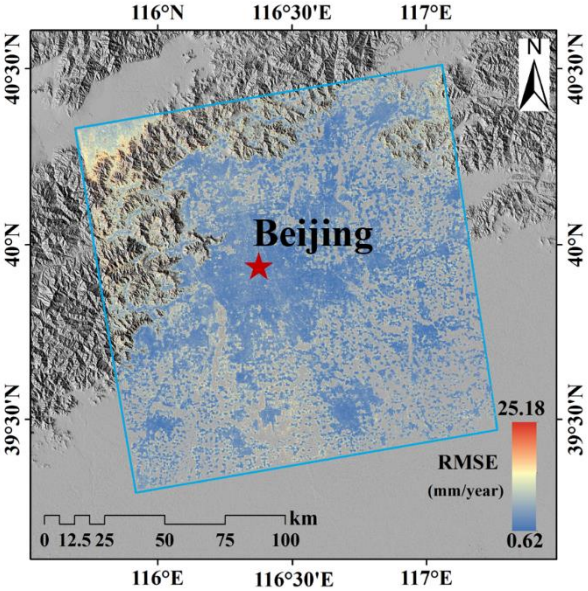

Figure 7. Distribution of RMSE in the study area

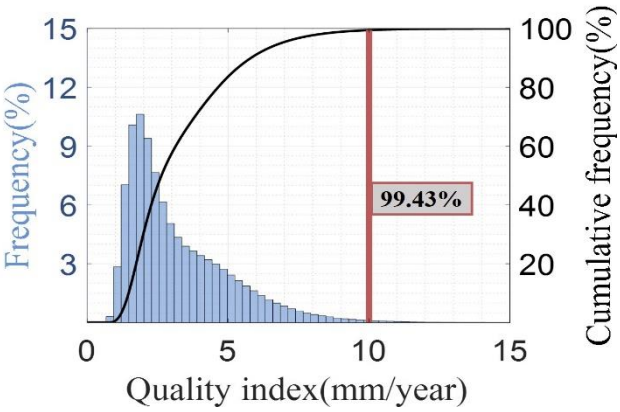

Figure 9. RMSE Statistical Histogram

5. Analysis and Discussion

5.1 Analysis of the Correlation Between Precipitation and Land Subsidence

To explore the influence of precipitation on land subsidence, this study utilized monthly precipitation data from the Beijing Plain during the monitoring period and time-series deformation information from the centers of three land subsidence areas for a comprehensive analysis. Figure 10 shows that the precipitation in the study area exhibits significant seasonal variations, with the summer months experiencing considerably higher rainfall than other months, minor precipitation in spring and autumn, and almost no rainfall in winter. According to the time-series visualization line segments of the three feature points, all three points exhibit linear surface deformation, with the land subsidence in these areas gradually intensifying over the study period.

The time-series surface deformation trends of the CY and TZ points are similar, and the influence of precipitation on the surface deformation at these two points can be directly observed from the figure. During the rainy season from May to September each year, a noticeable rebound in land subsidence occurs at both points, likely due to precipitation replenishing groundwater and causing a certain degree of ground uplift. After each rainy season, the slope of the surface deformation curves at these two points increases rapidly, a phenomenon that may be related to the accelerated land subsidence following the rapid decline in groundwater levels due to decreased precipitation. The time-series surface deformation curve of the YJ point also exhibits the aforementioned characteristics, but the impact of precipitation on the surface deformation at YJ point is less significant. The land subsidence in this area is also influenced by other factors.

The YJ point is located in Yanjiao Town, Hebei Province, bordering Beijing. According to the '2022 Hebei Province Water Resources Bulletin' published by the Hebei Provincial Department of Water Resources, the shallow groundwater level in the area of Yanjiao Town decreased by 0.5 meters in 2022, which might have significantly influenced the land subsidence status at the YJ point. The YJ point is located in Yanjiao Town, Hebei Province, bordering Beijing. According to the '2022 Hebei Province Water Resources Bulletin' published by the Hebei Provincial Department of Water Resources, the shallow groundwater level in the area of Yanjiao Town decreased by 0.5 meters in 2022, which might have influenced the land subsidence status at the YJ point. A comprehensive analysis combining the time-series deformation of the feature points with precipitation data reveals that all three points experience varying degrees of surface subsidence rebound during months with higher precipitation. The subsidence at TZ and CY points is more significantly affected by precipitation, while the YJ point is relatively less influenced by precipitation compared to TZ and CY points.

To quantitatively analyze the correlation between the time-series deformation of the three feature points and precipitation, this study employed the Grey Relation Analysis method (Huang et al., 2008) to calculate the correlation value between the time-series deformation data of the three points and precipitation. The correlation values for TZ, CY, and YJ are 0.77, 0.77, and 0.74, respectively. These results demonstrate a strong correlation between surface deformation at these three feature points and precipitation.

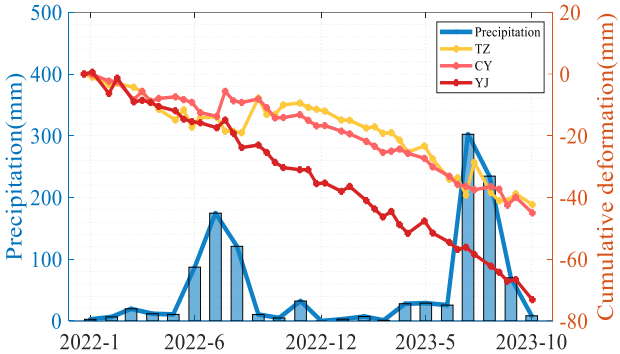

Figure 10. Analysis of precipitation and time-series surface deformation

5.2 Analysis of the impact of urban construction on land subsidence

Subsidence Area A is situated in the eastern part of Chaoyang District in Beijing, encompassing regions including Jinzhan Township, Caogezhuang Village, Ligezhuang Village, Magezhuang Village, among others. According to the 'Chaoyang District Subdivision Plan (Land and Space Planning) (2017-2035)' report, most areas in the eastern part of Chaoyang District are designated as concentrated construction zones. Among these, the Jinzhan International Cooperation Service Area is a region that has been vigorously developed by Chaoyang District in recent years. The concentrated construction zones require moderately advanced and prioritized development of transportation infrastructure, as well as the simultaneous improvement of urban infrastructure. Urban construction activities in this area might be one of the causes influencing land subsidence in the region. To verify this hypothesis, this paper selected two subsidence areas in Jinzhan Township and Ligezhuang for in-depth analysis (Figure 11). Through the comparative analysis of optical images at the inception and conclusion of the monitoring period, this paper discerned notable alterations in the surface structures within the land subsidence zones, with certain areas exhibiting ongoing renovation and reconstruction activities. Regions with construction activities exhibit a land subsidence rate exceeding −20 mm/year. The analysis confirms a significant correlation between land subsidence in Subsidence Area A and urban construction. The Jinzhan International Cooperation Service Area, recognized as a key component of Beijing's 'Two Zones' initiative, is a notably developed sector in the Chaoyang District. Given its high population density and the intensity of economic and trade activities, this area could be a contributing factor to the land subsidence phenomena observed in the region.

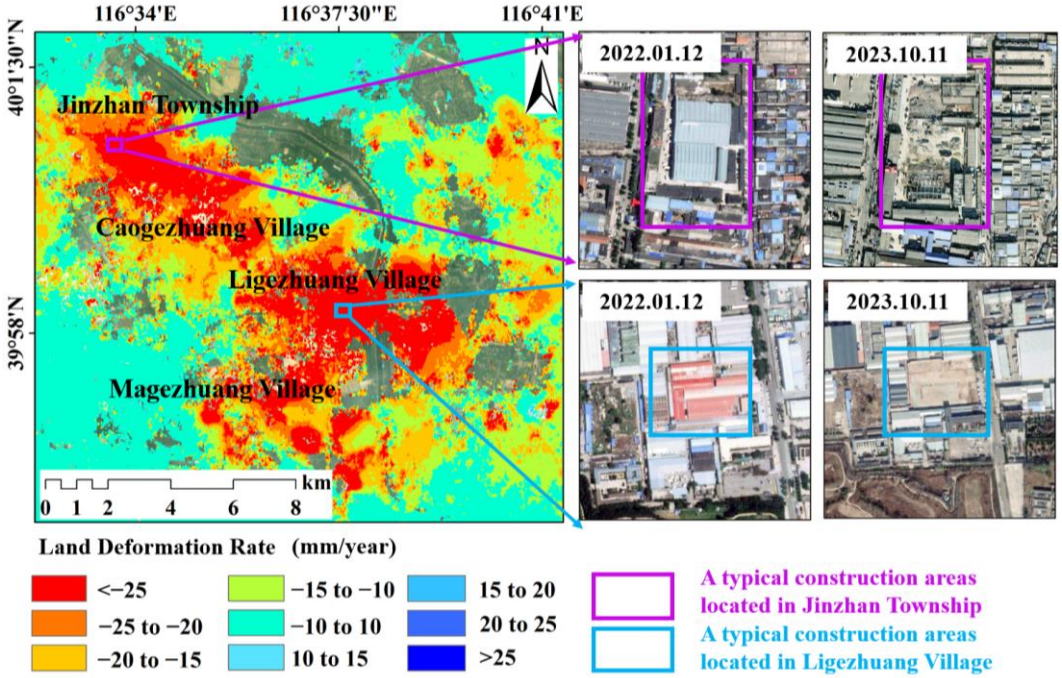

Figure 11. Comparative Analysis of subsidence Area A and Urban Construction (The purple box area represents the changes of a building site located in Jinzhan Township before and after the study period, while the blue box area represents the changes of a building site located in Ligezhuang before and after the study period)

Subsidence Area B is located in the northwestern region of Tongzhou, Beijing. The land subsidence in this area is relatively dispersed, with the main land subsidence occurring in Liyuan Town and Taihu Town. According to the 'Beijing Urban Sub-Center Detailed Control Plan (Block Level) (2016-2035),' it is indicated that a portion of the land subsidence area coincides with Beijing's Urban Sub-Center. The rapid development and construction of Beijing's Urban Sub-Center may potentially contribute to land subsidence in this area. Figure 12 compares optical images from January 2022 and October 2023 for two areas with significant land subsidence: Xixiaying Village and Shuinan Village. In these images, significant changes in surface structures are clearly observable. In the purple regions, existing buildings were demolished and replaced with new structures. The two blue areas represent completed reconstructions and ongoing surface construction. Through comparative analysis of optical images, this study suggests that urban construction has contributed to land subsidence in Zone B to some extent.

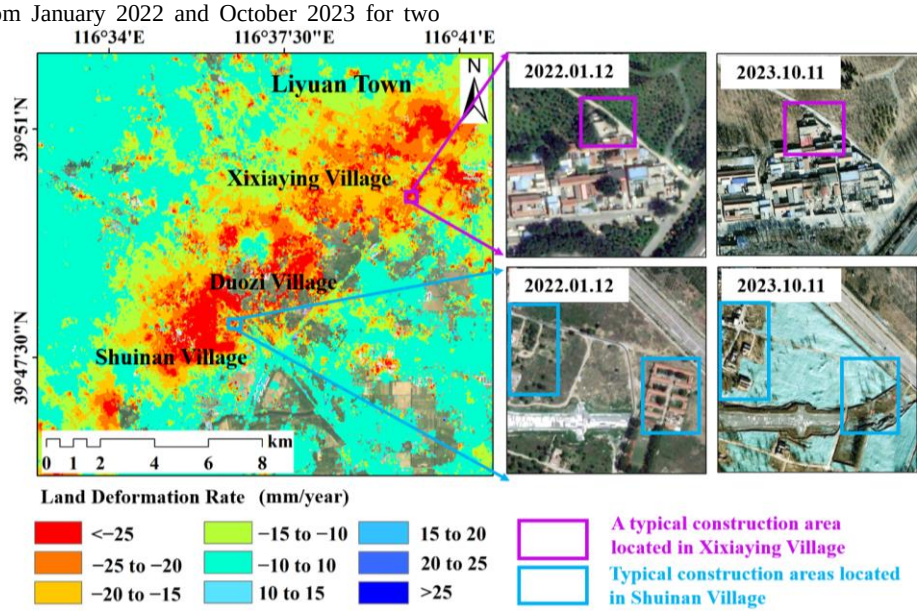

Figure 12. Comparative Analysis of subsidence Zone B and Urban Construction (The purple box area represents the changes of a building site located in Xixiaying Village before and after the study period, while the blue box area represents the changes of two building sites in Shuinan Village before and after the study period)

This contribution has been peer-reviewed. The double-blind peer-review was conducted on the basis of the full paper.
https://doi.org/10.5194/isprs-annals-X-1-2024-233-2024 | © Author(s) 2024. CC BY 4.0 License.

6. Conclusion

This article is based on SBAS InSAR technology and uses 43 Sentinel-1A images covering the study area from January 2022 to October 2023 to obtain surface deformation information in the Beijing Plain. The causes of land subsidence are analyzed through precipitation and urban construction. The research findings obtained in this study are as follows: (1) There are three distinct land subsidence areas in the Beijing Plain, located in the eastern part of Chaoyang District, Beijing (Subsidence Area A), the northwest part of Tongzhou District, Beijing (Subsidence Area B), and Yanjiao Town, Hebei Province (Subsidence Area C). The land subsidence in both Subsidence Area A and Subsidence Area B appears to be scattered, with the maximum land subsidence in both areas exceeding −30 mm/year. Subsidence Area C exhibits a distinct funnel-shaped land subsidence pattern, with the majority of the area experiencing land subsidence rate exceeding −25 mm/year, and the maximum land subsidence rate reaching −45 mm/year. (2) Precipitation has a significant impact on the surface deformation in the study area. Correlation values of 0.77, 0.77, and 0.74 were obtained for the three areas, confirming a strong correlation between precipitation and land subsidence. (3) Urban construction has an impact on land subsidence in the study area, but the degree of influence varies in different regions. The land subsidence in Chaoyang District and Tongzhou District is significantly influenced by urban construction.

Acknowledgements

The authors gratefully acknowledge the following organizations for their contributions to the research:
The Copernicus Program of the European Space Agency (ESA) (https://www.copernicus.eu) for freely supplying Sentinel-1A SAR images.
The United States Geological Survey (USGS) for providing the Shuttle Radar Topography Mission digital elevation model (SRTM DEM).
Additionally, we express our deep gratitude for the financial support from the following funding sources:
National Natural Science Foundation of China [grant number 42264004].
The Project Supported by the Open Fund of Hubei Luojia Laboratory [grant number 230100018].
Natural Science and Guangxi universities’ 1,000 young and middle-aged backbone teachers training program.
Funded by the Key Laboratory of China-ASEAN Satellite Remote Sensing Applications，Ministry of Natural Resources of the people's Republic of China.
Supported by Hubei Provincial Natural Science Foundation of China [grant number 2022CFB090].

References

Bagheri, M., Hosseini, S.M., 2021. Ataie-Ashtiani B, et al. Land subsidence: A global challenge. Science of The Total Environment, 778(6),146193.

Bamler, R., Hartl, P.,1998. Synthetic aperture radar interferometry. Inverse Problems, 14(4), R1-R54.

Berardino, P., Fornaro, G., 2002. Lanari R, et al. A New Algorithm for Surface Deformation Monitoring Based on Small Baseline Differential SAR Interferograms. IEEE Transactions on Geoscience & Remote Sensing, 40(11), 2375-2383.

Chen, B.B., Gong, H.L., Li, X.J., Lei, K.C., Zhu, L., Gao, M.L., Zhou, C.F., 2015. Characterization and causes of land subsidence in Beijing, China. International Journal of Remote Sensing, 38(3), 808-826.

Chen, M., Tomás, R., Li. Z., Motagh, M., Li, T., Hu, L., Gong, H., Li, X., Yu, J., Gong, X., 2016. Imaging Land Subsidence Induced by Groundwater Extraction in Beijing (China) Using Satellite Radar Interferometry. Remote Sensing, 8(6), 468.

Colesanti, C., Ferretti, A., Prati, C., Rocca, F., 2003. Monitoring landslides and tectonic motions with the Permanent Scatterers Technique. Engineering Geology, 68(1–2), 3-14.

Fattahi, H., Amelung, F., 2013. DEM Error Correction in InSAR Time Series. IEEE Transactions on Geoscience and Remote Sensing, 51(7), 4249-4259.

Ferretti, A., Prati, C., Rocca, F., 2001. Permanent scatterers in SAR interferometry. IEEE Transactions on Geoscience and Remote Sensing, 39(1),8-20.

Huang, S.J., Chiu, N.H., Chen, L.W., 2008. Integration of the grey relational analysis with genetic algorithm for software effort estimation. European Journal of Operational Research, 188(3), 898-909.

Sheng, H.Q., Zhou, L., Huang, C.J., Ma, S.B., Xian L.X., Chen, Y.K., Yang, F., 2023. Surface Subsidence Characteristics and Causes in Beijing (China) before and after COVID-19 by Sentinel-1A TS-InSAR. Remote Sensing, 15(5), 1199.

Tao, Q.X., Ding, L.J., Hu, L.Y., Chen, Y., Liu, T.W., 2020. The Performance of LS and SVD Methods for SBAS InSAR Deformation Model Solutions. International Journal of Remote Sensing, 41(22), 8547-8572.

Wang, Q., 2001. Present-Day Crustal Deformation in China Constrained by Global Positioning System Measurements. Science, 294(5542), 574-577.

Zhou, L., Guo, J.M., Li, X., Hu, J.Y., 2016. Monitoring and analyzing on ground subsidence in Beijing area based on SBAS-InSAR. J. Geod. Geodyn, 36, 793–797.